Title

The use of the bimodal production decline curve for the analysis of hydraulically fractured shale/tight gas reservoirs

Authors

Doughty, C
Moridis, GJ

Publication Date

2018

DOI

10.15530/urtec-2018-2903145

Peer reviewed

UNCONVENTIONAL RESOURCES TECHNOLOGY CONFERENCE
FUELED BY SPE • AAPG • SEG

URTeC: 2903145

The Use of the Bimodal Production Decline Curve for the Analysis of Hydraulically Fractured Shale/Tight Gas Reservoirs

Christine Doughty[1], George J. Moridis*[1,2]
1. Lawrence Berkeley National Laboratory, 2. Texas A&M University.

Abstract

The capability to conduct a rapid, near real-time model-based analysis of production data from tight/shale (TS) gas fields is important in determining fracture and matrix properties. Model-based analysis of production can range from simple analytical solutions to complex numerical models. The objective of this study is to develop a simple, Excel-based tool for the analysis of the complex problem of gas production from a fractured TS gas reservoir that is based on a robust model that is faithful to the underlying physics and can provide rapid estimates of the important system parameters.

The scientifically robust model used as the basis for this tool is a significant modification and expansion of the bimodal production decline curve of Silin and Kneafsey (2012). The production period is divided into two regimes: an early-time regime before the extent of the stimulated reservoir volume (SRV) is felt, where an analytical similarity solution for gas production rate is obtained, and a late-time regime where the rate can be approximated with an exponential decline or more accurately represented with a numerical integration. Our basic model follows Silin and Kneafsey (2012) and produces the widely observed -½ slope on a log-log plot of early-time production decline curves, while our expanded model generalizes this slope to $-n$, where $0 < n < 1$, to represent non-ideal flow geometries. The expanded model was programmed into an Excel spreadsheet to develop an interactive, user-friendly application for curve matching of well production data to the bimodal curve, from which matrix and fracture properties can be extracted.

This tool allows significant insight into the model parameters that control the reservoir behavior and production: the geometry of the hydraulically-induced fracture network, its flow and transport properties, and the optimal operational parameters. This information enables informed choices about future operations, and is valuable in several different ways: (a) to estimate

reserves and to predict future production, including expected ultimate recovery and the useful lifetime of the stage or the well; (b) if curve-matching is unsuccessful, to indicate the inadequacy of the mathematical model and the need for more complex numerical model to analyze the system; (c) to verify/validate numerical models, and to identify anomalous behavior or measurement errors in the data. The present approach can be adapted to gas-flow problems in dual-permeability media (hydraulically or naturally fractured) or highly heterogeneous sedimentary rock, as well as to retrograde condensation.

1. Introduction

1.1 Background

Hydrocarbon production from tight reservoirs has experienced explosive growth over the last few years. Gas production from shale and tight-sand deposits has proven remarkably successful in increasing substantially both gas production and reserves estimates in the U.S. In addition to its financial benefits, the development of technology to produce fossil fuels in previously inaccessible domestic geologic systems is considered a substantial contributor to energy security.

The universal feature of all tight reservoirs is the unavoidable need for well and reservoir stimulation: the matrix permeability is extremely low (often at the nano-Darcy level) and, even with the presence of a system of natural fractures, it cannot support flow at anything approaching commercially viable rates without permeability enhancement. Such enhancement/stimulation is provided by a number of methods, all of which are designed to develop a new system of artificial fractures that increase the permeability of the system and increase the surface area (over which reservoir fluids flow from the matrix to the permeable fractures) to provide access to a larger volume of the reservoir. Thus, stimulation techniques are the only means of rendering resource-rich but unproductive natural reservoirs into commercially viable entities. Fundamentally, it is stimulation technology that made gas and oil production from shales possible, and it is this same technology that has effected production increases of orders of magnitude over the last few years.

Conventional stimulation techniques are usually variants of hydraulic fracturing (King, 2012), in which the near-incompressibility of liquids is exploited to deliver a shock that induces rock fracturing stemming from the target point. In this case, the artificial fracture system is induced by the injection of water or of a water-based fluid into the fractures and the matrix of the geologic medium. The fracture system resulting from conventional stimulation is dominated by the “primary” fractures (planar or dendritic) that occur at the locations of stimulation treatment, which are surrounded by a network of smaller fractures making up the so-called stimulated reservoir volume (SRV) from which gas is produced.

Hydraulic fracturing of tight shale-gas formations greatly improves production, but there is a need for greater understanding of the ensuing reservoir fluid flow and production from the complex fractured system resulting from such reservoir stimulation. The production rate in hydraulically fractured wells generally declines quickly, necessitating additional fracture stages (a re-fracturing process) or new wells, both of which are expensive and carry increased environmental-impact risks. The complexity of the geologic systems resulting from the hydraulic fracturing of gas-bearing shales, coupled with the strong non-linearity of the flow of the highly compressible natural gas through the interacting fracture-matrix continua, create significant challenges in the analysis of production data because of the difficulty of extracting the necessary data describing the system properties. These are crucial for understanding the fracture characteristics (geometry, extent, aperture, orientation, etc.) and their effect on matrix-fracture mass exchanges. Such knowledge can provide a greater understanding of the flow geometry in the SRV, leading to improved estimates of expected production and a more accurate assessment of reserves and recoverable resources. Such knowledge can also offer guidance for additional/subsequent hydraulic fracturing operations, as well as important insights that have the potential to help design enhanced fracturing processes that minimize costs, water usage, drilling footprints, and other associated environmental concerns.

1.2. Statement of the Problem, Objective and Approach

To obtain the necessary knowledge on the fracture and matrix properties, it is necessary to have the capability to conduct a rapid, near real-time model-based analysis of data collected during production from tight/shale gas fields. Depending on the complexity of the system under investigation, model-based analysis of oil and gas production can range from simple analytical solutions to complex numerical models. Often, the complexity of fractured media with strong non-linear flows and significant pressure and temperature gradients preclude the use of simple analytical models, leaving numerical models as the only option. Such an endeavor is time-consuming, expensive, and requires experienced modelers (e.g., Olorode et al., 2012; Wang et al., 2013; Cai et al., 2015). It is therefore worthwhile, if the system under investigation lends itself to valid linearizations and approximations without violating basic laws of physics, to begin the analysis in a much simpler way, using an idealized representation of the real problem. The objective of this study is to develop a simple, Excel-based tool for the analysis of the complex problem of gas production from a hydraulically fractured tight/shale gas reservoir that is based on a model that remains faithful to the underlying physics and can provide rapid estimates of the important parameters governing the system behavior. Of the many analytical and semi-analytical solutions for gas production from hydraulically fractured tight/shale gas reservoirs that have been developed in the past decade (e.g., Ilk et al., 2008; Al-Ahmadi et al., 2010; Nobakht and Clarkson, 2011; Silin and Kneafsey, 2012; Patzek et al., 2013, 2014; Lunati and Lee,

2014), some miss essential physics (in particular, addressing both early-time behavior when the SRV is infinite acting and late-time behavior when its boundaries are felt) and others are too complex for ready implementation in a spreadsheet.

The starting point for this work is the scientifically robust model of Silin and Kneafsey (2012), hereafter referred to as S&K, which yields a semi-analytical solution for a bimodal production decline curve, incorporating both early- and late-time behavior. S&K includes a complete description of the processes modeled, the assumptions employed, and the derivation of their semi-analytical solution, which will not be repeated here, except for a few equations that contained errors, for which corrected versions are given in Appendix A. Although it includes a one-dimensional numerical integration, this solution is amenable to spreadsheet implementation, and we programmed the S&K solution into an Excel spreadsheet and developed an interactive, user-friendly, Excel-based application for curve matching of well production data to the bimodal curve, by varying the aggregate (composite) variables defined in S&K. In a second step, the individual matrix and fracture properties that compose the aggregate variables can be extracted. In so doing, we can gain significant insight into the model parameters that control gas production: the geometry of the hydraulically induced fracture network, its flow and transport properties, and the optimal operational parameters.

In addition to providing the information on the induced fracture network needed to make informed choices about future operations, the curve-fitting process is valuable in several different ways. First, curve fitting is essentially history matching, so a calibrated model can then be used to predict future production rate, including expected ultimate recovery and the useful lifetime of the stage or the well. Second, if curve fitting is not successful, that is, if no combination of aggregate parameters can provide an acceptable match between the data and the bimodal curve, this indicates that the real system is not behaving as predicted by the idealized mathematical model and, therefore, that the assumptions of the idealized model are not met. In that case, the use of a more complex numerical model to analyze the system is the only recourse. The semi-analytical solution is also useful as a reference for the verification/validation of numerical models. Finally, if the bulk of the production data can be represented by the bimodal curve, then data points that do not fit the curve suggest local or short-term anomalous behavior or measurement error.

This paper is organized as follows. In Section 2, the idealized problem and the S&K semi-analytical solution are introduced, along with the Excel spreadsheet methodology. Section 3 illustrates the results of the curve-fitting procedure with an example problem. Section 4 discusses the motivation for, concept behind, and general features of the expanded model with early-time slope generalized from -½ to $-n$, and illustrates its use on an example problem. Section 5 provides concluding remarks.

2. Method

2.1. Assumptions

The S&K problem is illustrated in Figure 1, which shows several fracture stages along a horizontal well. Each fracture stage consists of a SRV of thickness $2D$, consisting of a planar primary fracture of areal extent A perpendicular to the wellbore and a network of smaller secondary fractures orthogonal to the primary fracture. It is assumed that for a tight gas reservoir, production only occurs from the SRV. Additionally, it is assumed that the permeability of the primary fracture is so great that the pressure in the primary fracture is uniform and equals the pressure in the well. Hence the semi-analytical solution only models flow through the orthogonal fracture network. The solution can be applied to the SRV resulting from a single hydraulic fracture stage or to multiple SRVs resulting from identical stages that were created simultaneously, in which case A would be the sum of the areal extents of all stages.

The fluid is assumed to be single-phase, constant-compressibility gas, which flows according to Darcy's law, and is in equilibrium with gas adsorbed on the rock (for more details, see S&K). The system is assumed to remain at constant temperature, and all thermophysical properties, such as density, viscosity, and sorption coefficient, are a function of pressure only. Initially, the gas in the reservoir and the well is at a constant pressure, p_R; at time zero the pressure at the well is dropped to p_W, where it is held constant during the production process.

2.2. S&K Bimodal Solution for Production Decline Curve

The production period is divided into two regimes: An early-time regime before the extent of the SRV is felt, where an analytical similarity solution for gas production rate can be obtained, and a late-time regime where the rate can be approximated with an exponential decline, or more accurately with a semi-analytical solution obtained by numerical integration. The key parameters controlling the solution are characteristic time t_0, characteristic flow rate Q_0, and parameter u_0, which is the square of the ratio of well pressure to reservoir pressure and which determines the transition time between early-time and late-time regimes t^*.

The solution for dimensionless production rate $Q_D = Q/Q_0$ as a function of dimensionless time $\tau = t/t_0$ and parameter u_0 is given by S&K Eq. (A-13) as

$$Q_D = \frac{2(1-u_0)}{\alpha \tau^{1/2}} \qquad \text{for} \quad \tau < \frac{1}{\alpha^2} \tag{1a}$$

$$¿ 2\beta(\tau)(1-u_0) \qquad \text{for} \quad \tau > \frac{1}{\alpha^2}\ , \tag{1b}$$

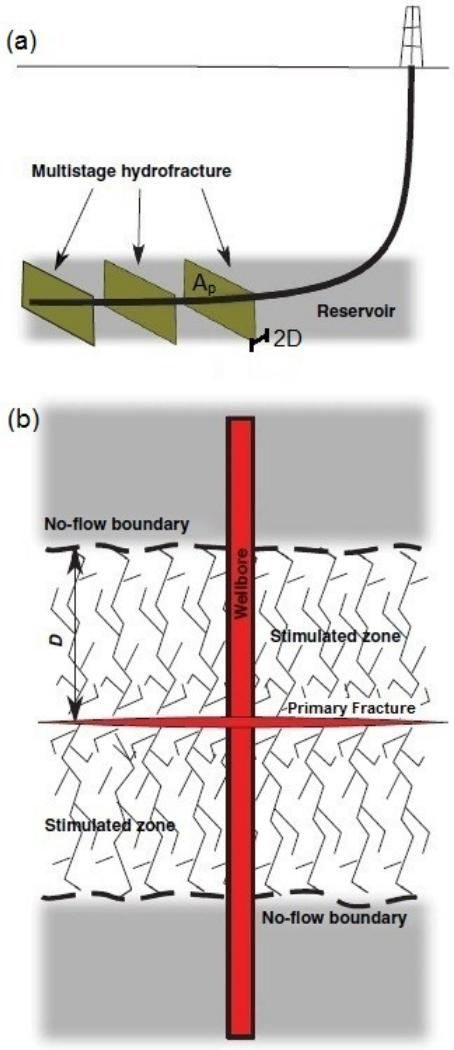

Figure 1 — Schematic of the idealized problem (modified from Silin and Kneafsey, 2012).

where $\beta(\tau)$ is the solution of the ordinary differential equation given by S&K Eq. (A-9)

$$\frac{d\beta(\tau)}{d\tau}=\frac{-3}{2}\beta(\tau)\sqrt{u_0}\left[1+\frac{u_0+\beta(\tau)(1-u_0)}{\sqrt{\beta(\tau)(1-u_0)u_0}}\arctan\sqrt{\frac{\beta(\tau)(1-u_0)}{u_0}}\right] \quad . \tag{2}$$

For small values of β, Equation (2) can be approximated as S&K Eq. (A-12)

$$\beta(\tau)=\exp\left[-3\sqrt{u_0}\left(\tau-\frac{1}{\alpha^2}\right)\right]. \tag{3}$$

The parameter α is given by S&K Eq. (A-8) as

$$\alpha=\sqrt{6\left(\sqrt{u_0}+\frac{1}{\sqrt{1-u_0}}\arcsin\sqrt{1-u_0}\right)}. \quad (4)$$

Figure 2 shows a log-log plot of Q_D versus τ, for $u_0 = 0.5$. Note that the early-time solution is linear with a slope of -½, as specified in Equation (1a). For late times, both the exponential approximation given by Equation (3) and the full solution given by numerical integration of Equation (2) are shown. The dimensionless transition time τ^* is given by

$$\tau^{*}=\frac{1}{\alpha^2} \quad (5)$$

and $\beta(\tau^*) = 1$ to assure continuity of Q_D at τ^*. The definitions of aggregate parameters u_0, t_0, and Q_0 are given by

$$u_0=\left(\frac{p_W}{p_R}\right)^2. \quad (6)$$

$$t_0=\left(1+\frac{\rho_0\rho_k S_k c_f}{c_g\phi}\right)\frac{\mu\phi D^2}{k_D p_R} \quad (7)$$

$$Q_0=\frac{A c_g k_D p_R^2}{\rho_0\mu D} \quad (8)$$

See Nomenclature for a definition of all variables.

Figure 3 shows Q_D versus τ for a range of u_0 values. As u_0 gets smaller (well pressure fixed at a smaller fraction of reservoir pressure), production rate increases. The dimensionless transition time τ^* and the curvature of the late-time solution depend weakly on u_0, but the early-time slope is always -½. (In the Discussion section below, we consider early-time slope to be a variable, -n, that can be fit to observed pressure decline.) Figure 3 indicates that the approximate exponential solution for late-times is not a very good approximation for small values of u_0, indicating that in general the numerical integration of Equation (2) is required to obtain $\beta(\tau)$ and hence Q_D.

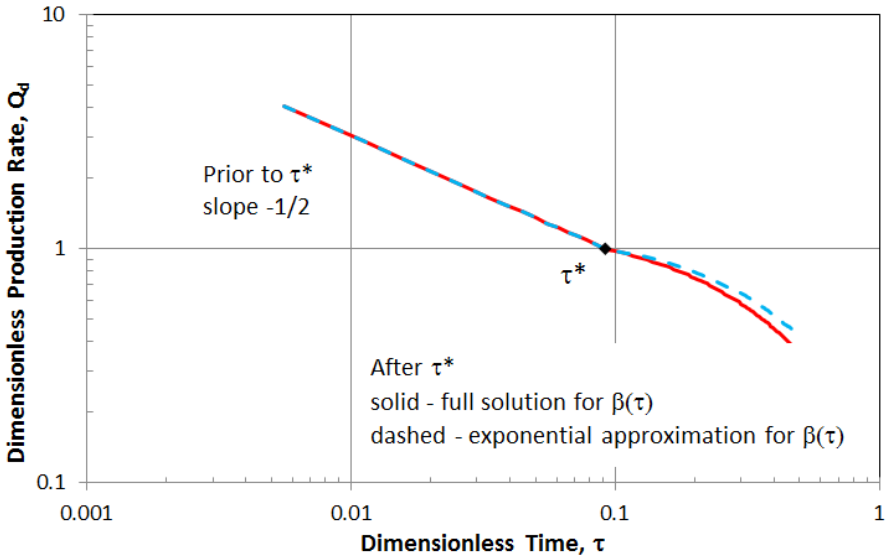

Figure 2 — S&K bimodal solution: prior to τ*, solution is given by Equation (1a), after τ* solutions are given by Equation (1b) with β obtained from Equation (2) (solid line) or Equation (3) (dashed line). Dimensionless transition time τ* is shown by the black diamond.

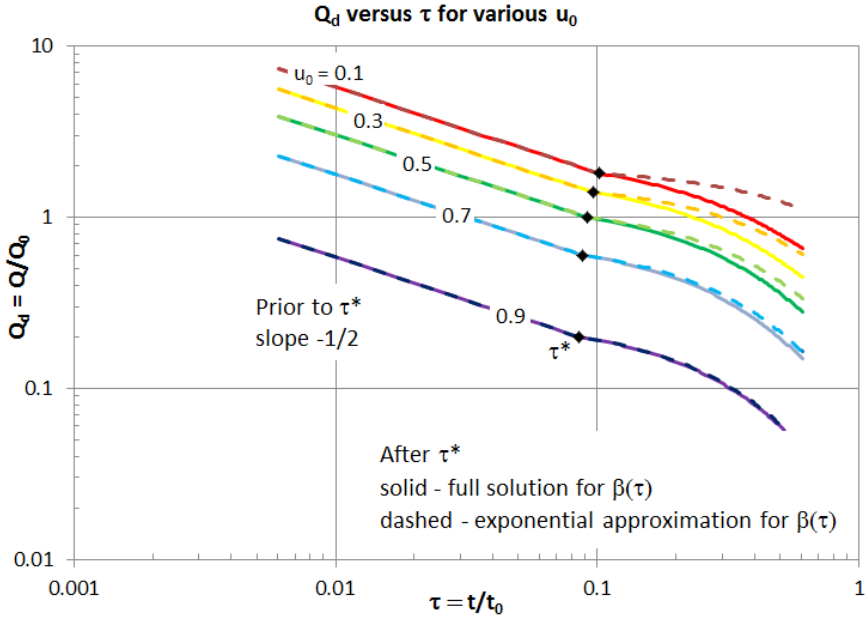

Figure 3—S&K bimodal solution for a range of values of u_0.

2.3. Excel Spreadsheet for Curve-Fitting

The semi-analytical S&K solution for the production rate that is given by Equations (1) - (8) was programmed into an Excel spreadsheet. The function β(τ) for the S&K late-time solution (Equation 1b) is obtained by numerical integration using a fourth-order Rung-Kutta algorithm from Numerical

Recipes (Press et al., 1986). The exponential approximation (Equation 3) is also shown for comparison, but it is not used for fitting. Figure 4 shows a screenshot of the spreadsheet. A detailed user's guide for the spreadsheet (Doughty and Moridis, 2018) is currently being finalized.

Curve fitting is accomplished in two steps: first, the aggregate variables are determined by matching modeled production decline curves to field data. Second, the individual parameters that comprise the aggregate variables are determined. Both steps of the curve-fitting process can be executed by trial and error or automatically using the Solver tool in Excel. Before attempting automated curve fitting, it is strongly recommended to first use the trial and error approach in each step of the curve-fitting process in order to gain experience with the sensitivity of the solution to different parameters and to determine reasonable initial guesses of unknown parameters. As in any application of an inverse method (i.e., in history matching), it is a sound practice to repeat the fitting process using different initial guesses for the various parameters to assess the possibility of non-uniqueness of the solution.

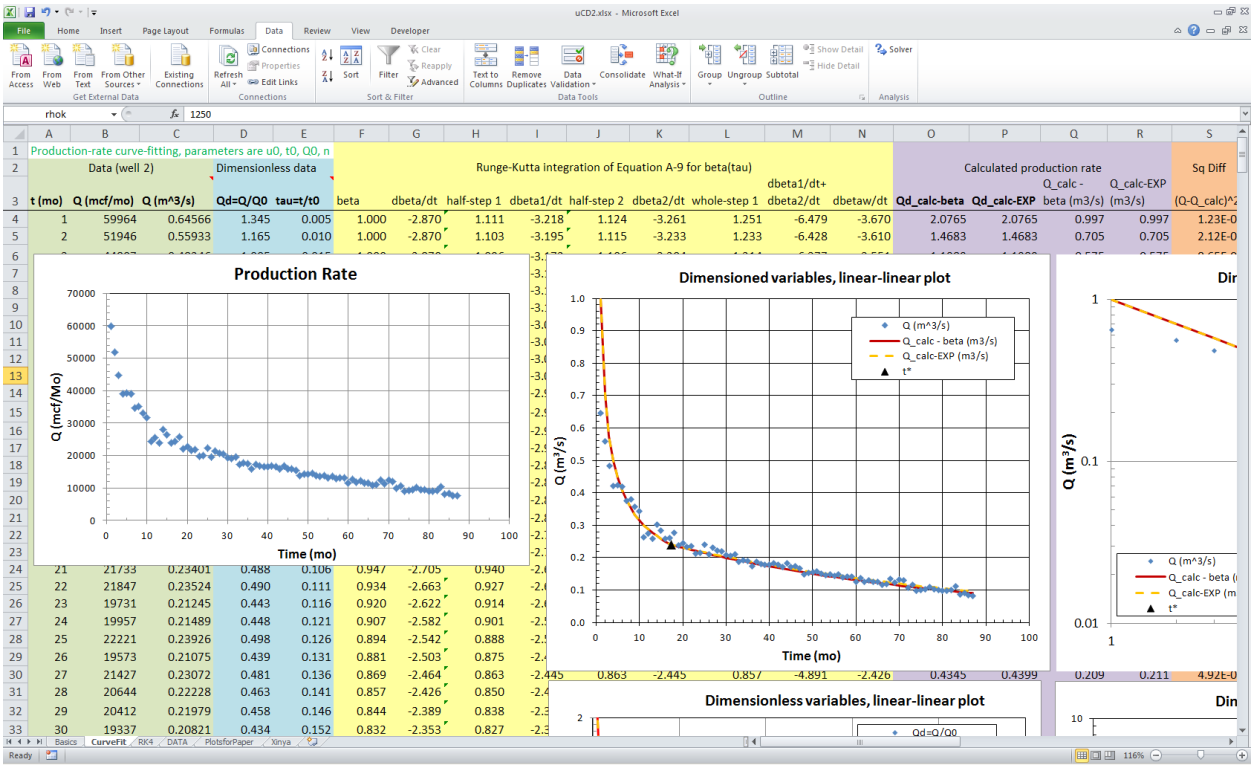

10

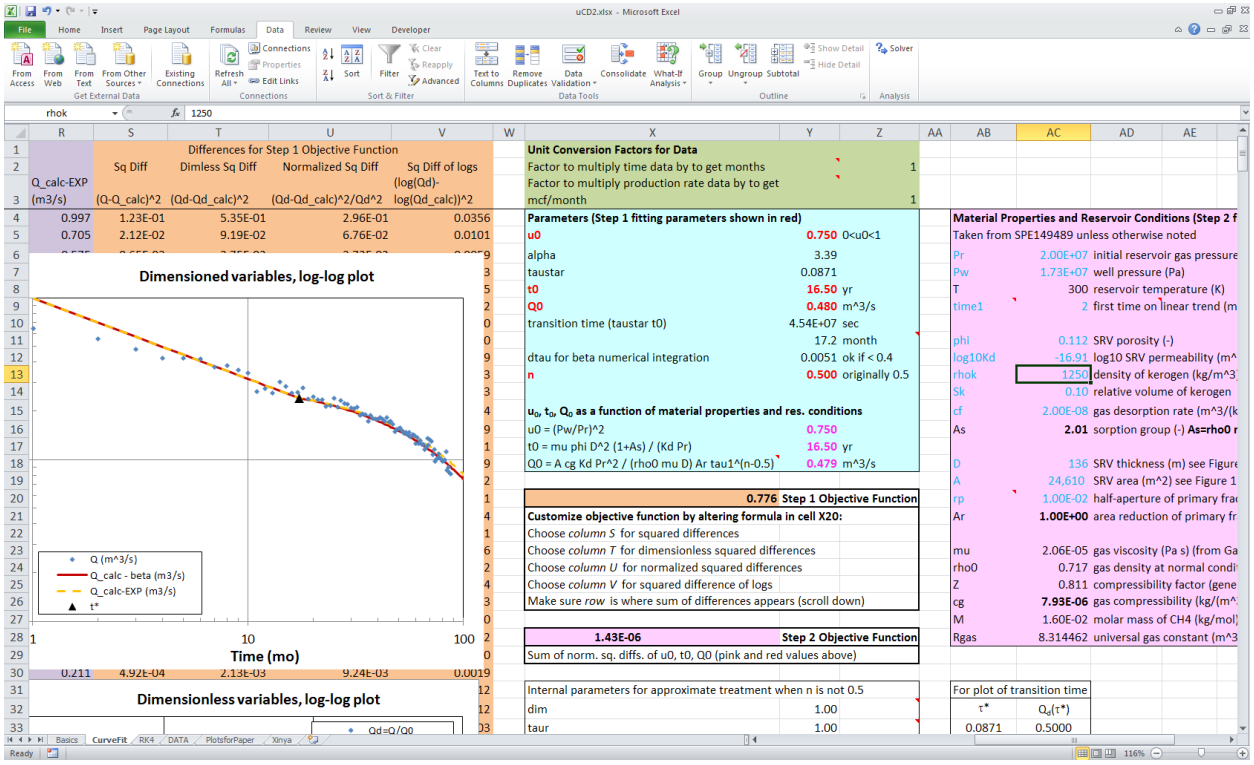

Figure 4—Screen shots of the Excel spreadsheet tab or curve fitting.

Step 1 – Fitting Aggregate Variables

The aggregate variables u_0, t_0, and Q_0 are the unknown parameters, and the objective function to be minimized is the sum of squared errors between the modeled production decline curve and the data. The parameter n should be set to ½ so that the model represents Equation (1a) for the S&K early-time solution. Note that on a log-log plot, changing t_0 and Q_0 will merely shift the decline curve along the horizontal and vertical axes, respectively, whereas changing u_0 will change the shape of the curve, as shown in Figure 3.

Step 2 – Fitting Individual Variables

The material properties of the SRV (flow properties ϕ, k_D; sorption properties ρ_k, S_k, c_f), fracture geometry (A, D) and reservoir conditions (p_W, p_R) that determine the aggregate variables u_0, t_0, and Q_0, through Equations (6), (7), and (8) are the unknown parameters, and the objective function to be minimized is the sum of normalized squares differences between (a) the values of u_0, t_0, and Q_0 calculated with these parameters and (b) the values of the same variables that were determined in Step 1. For improved stability in the curve-fitting process, the log of permeability rather than permeability itself is used as an unknown parameter. With nine parameters and only three equations relating them, it is obvious that a unique solution is not possible, but if some of the parameters can be estimated from independent information, then the inversion can place useful constraints on other parameters, as illustrated in the example application below.

Other parameters that must be specified, but are not expected to be part of the fitting process, are the temperature T, the gas molar mass M, the gas viscosity μ, a reference gas density ρ_0, and the gas compressibility factor Z. Values of μ, ρ_0, and Z for pure gases and mixtures may be found from the GasEOS website (http://lnx.lbl.gov/gaseos/home.html). For small values of u_0, reservoir pressure p_R and well pressure p_W differ significantly. Early-time production rate is most sensitive to near-well conditions (p_W) whereas late-time production rate is most sensitive to far-field conditions (p_R). For fitting to the entire production curve, it is recommended to evaluate pressure-dependent properties μ and Z at both p_R and p_W and use the average. If p_W or p_R changes significantly from its initial guess during the fitting process, μ and Z should be reset.

Given the bimodal form of the production decline curve, it would seem appealing to use the transition time t^* or the dimensionless transition time τ^* directly as one of the unknown parameters instead of u_0 because τ^* only depends on u_0, through α (see Equations (4) and (5)). We investigated this option but rejected it as impractical because τ^* cannot be expressed explicitly as a function of u_0, and determining u_0 for a given τ^* would require an additional iterative loop within the optimization process. However, within the Excel Solver tool, it is possible to apply constraints on parameters during the optimization, and a constraint on t^* or τ^* can be imposed, even if it is not one of the unknown parameters. Thus, if the production data show a definite

signature of a transition between early-time and late-time behavior at a given time, that time can be held fixed during the optimization for parameters u_0, t_0, and Q_0.

3. Results

To illustrate the method and the Excel tool, we use the production data shown in Figure 9 of S&K. The data set consists of 87 monthly measurements.

For Step 1, the initial values of u_0 = 0.75, t_0 = 10 years, and Q_0 = 0.4 m^3/s (left over from a previous problem) produce a poor match to the data (Figure 5) and a value of 18.7 for the objective function. We assume that u_0 is known. A few trial and error adjustments of the inputs to t_0 = 11 years, Q_0 = 0.6 m^3/s, yields a better match and a value of 2.9 for the objective function. This is the starting point for the automatic curve fit with the Solver. The Solver returns t_0 = 16.5 years, and Q_0 = 0.48 m^3/s, and a value of 0.78 for the objective function. The curve fit, shown in Figure 8, over-estimates production corresponding to the first four time-data points, but is very good for all times after 4 months.

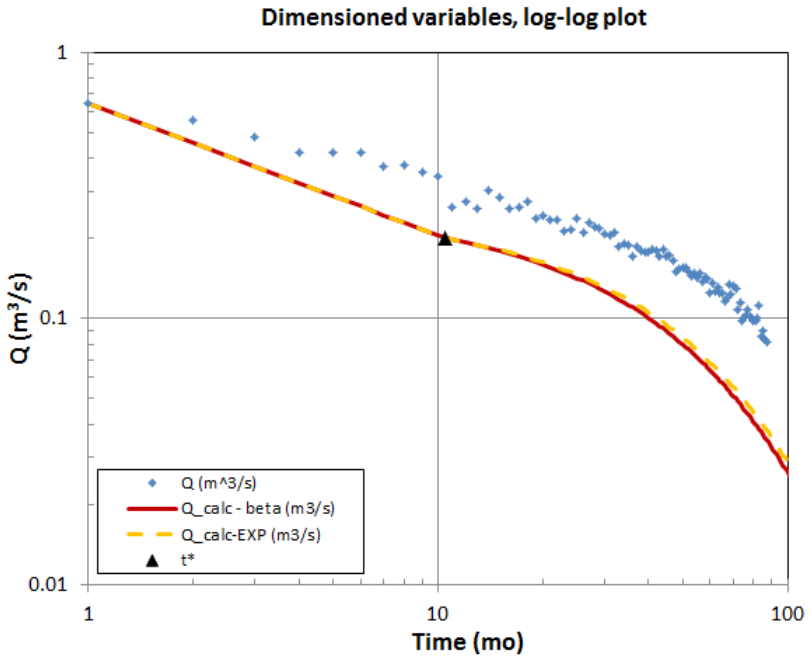

Figure 5—Production decline curves for data (symbols, taken from S&K Figure 9) and model (lines) using poor initial guesses for parameters.

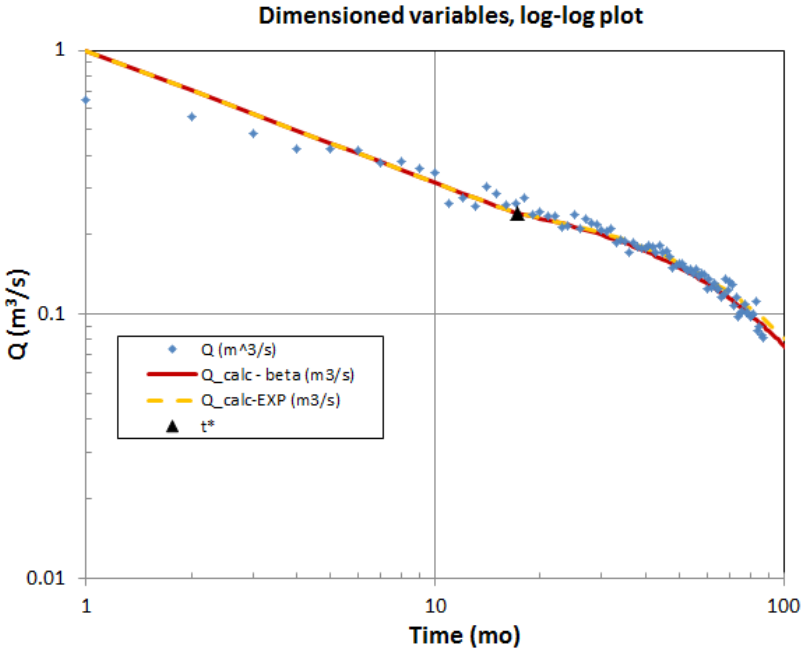

Figure 6—Step 1 curve-fit obtained by the Solver.

For Step 2, we assume that the reservoir pressure p_R is known, so the well pressure p_W can be immediately determined from u_0, as $p_W = u_0^{1/2} p_R$. For u_0 = 0.75 and p_R = 200 bars, p_W =173 bars. We focus on the flow properties ϕ and k_D, and the fracture geometry parameters D and A. The initial guesses (taken from another problem) are ϕ = 0.12, $\log_{10} k_D$ = -16.90 (k_D = 1.26E-17 m^2 = 0.013 mD), D = 167 m, and A = 30000 m^2. The Solver output matches the Step 1 values of t_0 and Q_0 closely, yielding an objective function of 4.6E-9, and returns parameter values of ϕ = 0.11, $\log_{10} k_D$ = -16.98 (k_D = 0.01 mD), D = 124 m, and A = 26754 m^2. These values are all physically reasonable. However, if an order of magnitude smaller porosity value (0.01) is used as an initial guess, the Solver obtains an equally good match (objective function 1.7E-6), returning ϕ = 0.01, $\log_{10} k_D$ = -16.91 (k_D = 0.012 mD), D = 163 m, and A = 29353 m^2. Note that these values of k_D, D, and A are not very different from the values returned for ϕ = 0.1, implying that within this range, the solution is not very sensitive to porosity. This lack of sensitivity can be verified by examining Equation (7) for t_0. When ϕ is small, the second term within the parenthesis is large, and the ϕ terms in t_0 cancel out. In contrast, if the k_D value used as an initial guess is 100 times larger or 100 times smaller, the Solver returns solutions with similar values for all parameters, as shown in Table 1, indicating that the solution is sensitive to k_D in this range. Varying the initial guess of all parameters in this way can provide useful information on the reliability of the parameter values returned by the Solver.

4. Discussion of Expanded Solution for Early-Time Slopes of -*n*

The -½ early-time slope is considered universal by most production decline curve analyses (e.g., Patzek et al., 2013), and in fact it has been successfully applied to many wells and plays. Examining log-log plots of production decline curves from a small set of hydraulically-fractured shale-gas wells (Figure 7) shows that while most show a -½ slope at early time as embodied in the S&K solution (Eq. 1a), some do not. Detailed numerical simulations (Olorode et al., 2012) confirm this finding and indicate that one reason for different early-time slopes is non-ideal geometry of the primary fracture (e.g., primary fracture is not perpendicular to the well; primary fracture is non-planar), such that flow from the SRV to the primary fracture does not have the linear flow geometry assumed for the S&K solution (Figure 1).

Cinco-Ley and Samaniego (1981) studied the pressure response to constant-rate pumping from a reservoir intercepted by a higher-permeability vertical fracture, and showed that when flow from the reservoir to the fracture is uniform and one-dimensional (the "formation linear flow" period, which is equivalent to the assumptions of S&K), log-log pressure drop increases with a ½ slope, consistent with S&K. However, at earlier times when flow in the reservoir and flow in the fracture are both significant (the " bilinear flow" period) the slope is smaller, ¼, and at late times when flow is from the surrounding reservoir converges toward the fracture (the "pseudo radial flow" period), the slope is even smaller.

Table 1 – Step 2 results for different initial guesses of $\log_{10}k_D$. In all cases initial guesses for other parameters are ϕ = 0.12, D = 167 m, A = 30,000 m^2.

Initial guess for $\log_{10}k_D$	Objective function	ϕ	$\log_{10}k_D$ (k_D in m^2)	D (m)	A (m^2)
-14.9	4.7E-8	0.113	-16.89	138	24140
-16.9	4.6E-9	0.113	-16.98	124	26754
-18.9	1.4e-6	0.112	-16.91	136	24610

Barker (1988) conducted well-test analyses for infinite reservoirs with flow dimension d ranging from 1 to 3, where d = 1 is linear flow to a planar sink (the geometry of the S&K problem), d = 2 is radial flow to a line sink, d = 3 is spherical flow to a point sink, and intermediate non-integer values of d are considered as well. His solutions show that when pressure change is plotted as a function of time on a log-log plot, the late-time response is linear with a slope that depends on d. For d = 1, slope is ½, and as d increases, slope decreases according to 1 – d/2, until for $d \geq 2$, slope is zero (i.e., steady-state pressure conditions prevail).

Observations from field data (Figure 7), along with the works of Olorode et al. (2012), Cinco-Ley and Samaniego (1981), and Barker (1988), motivate us to generalize the S&K solution so that the early-time slope can have a value -n other than being fixed at -½. This generalized solution is hereafter referred to as mS&K.

To obtain a physical interpretation of the parameter n, we consider Barker's finding that for constant-rate production from an infinite reservoir, the slope of the late-time pressure response depends on the flow dimension d. It seems plausible that the early-time slope of the bimodal production decline curve, before the boundary of the SRV is sensed by the system (i.e., when the SRV is infinite acting), is also controlled by d. For fractured rocks, the flow dimension d is determined by the fracture-network connectivity. Thus, we are hypothesizing that there is a quantitative relationship between the early-time slope of the production decline curve -n and the properties of the induced fracture network, as embodied in d.

The original case considered in S&K assumes $d = 1$, as gas flows uniformly through the SRV toward a planar primary fracture with uniform high permeability, as illustrated schematically in Figure 8b. Gas flow to the primary fracture has linear flow geometry, and this flow is uniform over the entire area of the fracture. However, if one considers a non-uniform primary fracture, with localized regions of high permeability, it is possible to imagine flow from the SRV converging to these portions of the fracture, yielding $d > 1$ (Figures 8c and 8d). In the extreme case of just one point on the primary fracture providing high permeability, with spherically symmetric flow from the SRV entering the facture at that one point, one would have $d = 3$. If quasi-linear regions of the primary fracture provided high permeability, with radial flow from the SRV entering the fracture along those lines, then one would have $d = 2$ (Figure 8d). Different patterns of localized high permeability in the primary fracture could produce non-integer values of $1 < d < 2$ (Figure 2c). On the other hand, if the primary fracture had uniform, high permeability, but flow paths through the SRV were limited due to a sparse or poorly connected fracture network, then $d < 1$ would also be possible (Figure 8a).

Thus, we want to be able to analyze SRV's in which the fracture network has a flow dimension d ranging from less than one to near two. Following Barker's finding that $n = 1 - d/2$ for $d \leq 2$ and $n = 0$ for $d \geq 2$, this corresponds to $0 < n < 1$. To create a solution with an early-time slope of -n, where n can be adjusted to fit observed production decline data, we replace the exponent ½ in the denominator of Equation (1a) with n. The late-time solution is basically unchanged from the original S&K formulation (Eq. 1b), but the value and slope at the transition time are altered to be consistent with the early-time solution. Our original plan was to follow the same procedure as S&K: assume a trial form for the bimodal solution with unknown parameters α and β, substitute it into the governing equation (modified from the original one-dimensional version to a d-dimensional version), and integrate over the SRV to determine equations for α and β. However, this approach was not successful, so we resort to numerical simulations to verify our assumed functional form.

Numerical simulations described in Appendix B simulate gas production from fracture networks with different flow dimensions d ranging

from 0.25 to 3. Figure 9 compares the numerically simulated production decline curve for $d = 1$ and the S&K solution. After about one hour, the numerical simulation reproduces the early-time slope of -½ and matches the entire S&K bimodal decline curve quite well, verifying that the numerical simulation correctly represents the original S&K problem.

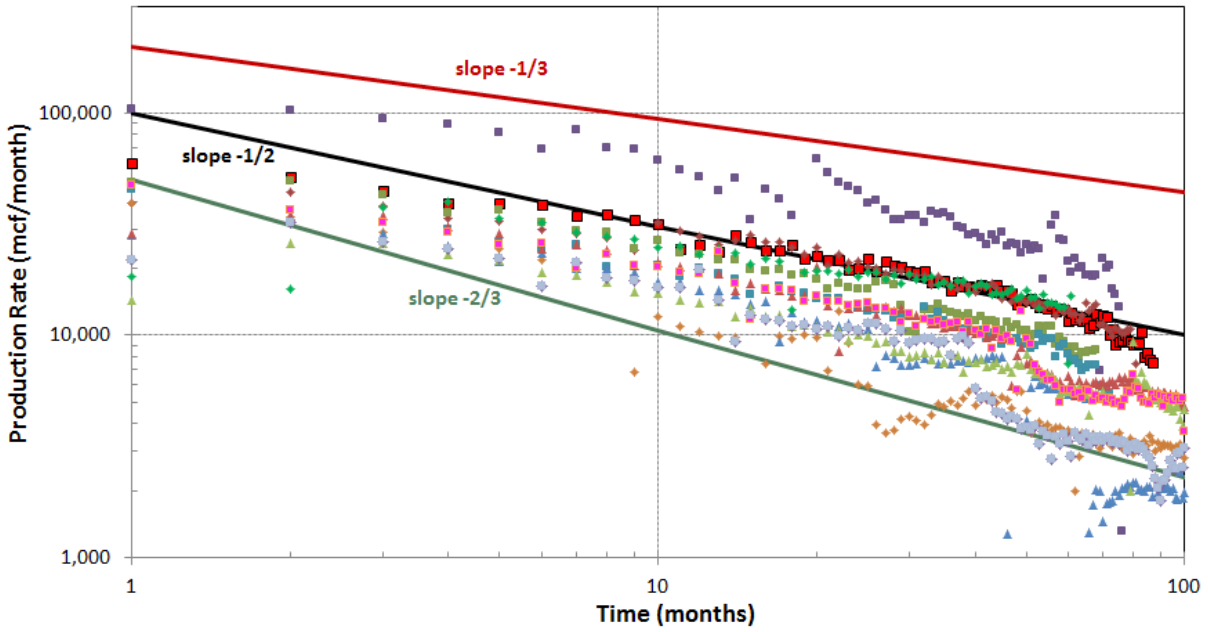

Figure 7 — Production decline data (symbols) from shale-gas wells (Texas Railroad Commission data). Log-log slopes of 1/3, 1/2, and 2/3 are also shown (lines).

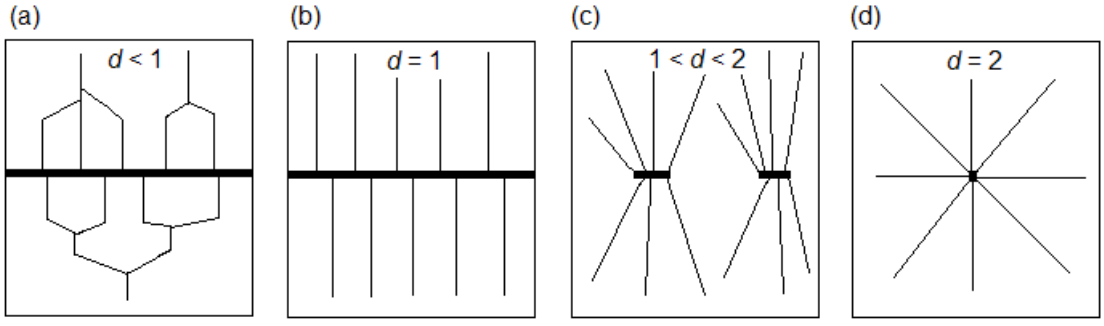

Figure 8 — Schematic diagrams of flow from fracture network (thin lines) to high-permeability regions of the primary fracture (thick lines), showing (a) diverging geometry for $d < 1$, (b) linear geometry for $d = 1$, (c) slightly converging geometry for $1 < d < 2$, and (d) strongly converting geometry for $d = 2$. The plots show a cross-section perpendicular to the plane of the primary fracture.

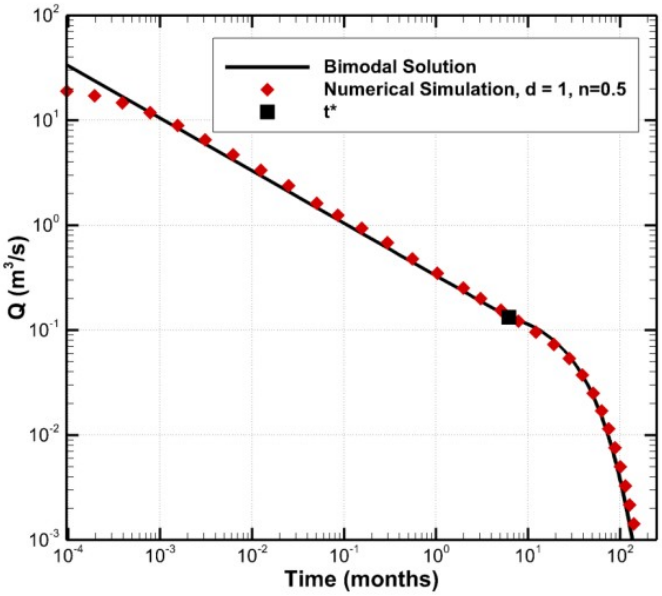

Figure 9 — Comparison of original S&K bimodal decline curve (line) and a numerical simulation for flow dimension d = 1 (symbols), for u_0 = 0.766. The early-time slope -n = -½.

Figure 10 shows numerically simulated production rate Q as a function of time on a log-log scale for various d values. All the curves for $d \leq 1$ (Figure 10a) show a linear portion with a slope $-n$, where $n = 1 - d/2$, that is established within an hour, and lasts until the pressure response reaches the outermost grid block of the column at $t = t^*$, after which Q declines more rapidly. For $1 < d \leq 3$ (Figure 10b), the outer boundary of the SRV is felt before the slope $-(1 - d/2)$ can be observed, but additional simulations with models of large radial extent (black dashed lines in Figure 10) show slopes of $-(1 - d/2)$ for $d < 2$, and slopes approaching zero for $d > 2$.

Several adjustments must be applied to the expanded bimodal solution to match the numerical simulation results. The first is a scaling factor that does not affect the shape of the production decline curve, but that translates the curves up or down to reflect the conceptual model of the area of the primary fracture: constant for $d < 1$ and decreasing with d for $d > 1$ (Figure 8). The second is to make τ^* dependent on d when $d > 1$, resulting in a later transition times as d increases. With these changes the expanded bimodal solution matches the numerical simulation results well for $d < 2$ (Doughty and Moridis, 2018). However, it cannot be used in its current form for $d \geq 2$.

In step 1 of the Excel spreadsheet application, the aggregate variables u_0, t_0, Q_0, and n are the unknown parameters, and the objective function to be minimized is the sum of squared errors between the modeled production decline curve and the data. On a log-log plot, changing t_0 and Q_0 will merely shift the decline curve along the horizontal and vertical axes, respectively, whereas changing u_0 and n will change the shape of the curve, as shown in Figure 3 and Figure 10, respectively. Because n controls mainly the early-

time slope, it can often be determined first and independently of the other parameters. In step 2, the material properties of the SRV (flow properties ϕ, k_D; sorption properties ρ_k, S_k, c_f), fracture geometry (A, D, r_p) and reservoir conditions (p_W, p_R, t_1) that determine the aggregate variables u_0, t_0, and Q_0 are the unknown parameters, and the objective function to be minimized is the sum of normalized squares differences between (a) the values of u_0, t_0, and Q_0 calculated with these parameters and (b) the values of the same variables that were determined in step 1. The only difference from the n = ½ case is the inclusion of two new individual variables: t_1, the earliest time the bimodal curve falls on a straight line, and r_p, the half-width of the primary fracture. The parameter t_1 can usually be determined by direct examination of the field data, and constraining information on r_p may be available from independent studies of the hydraulic fracturing process.

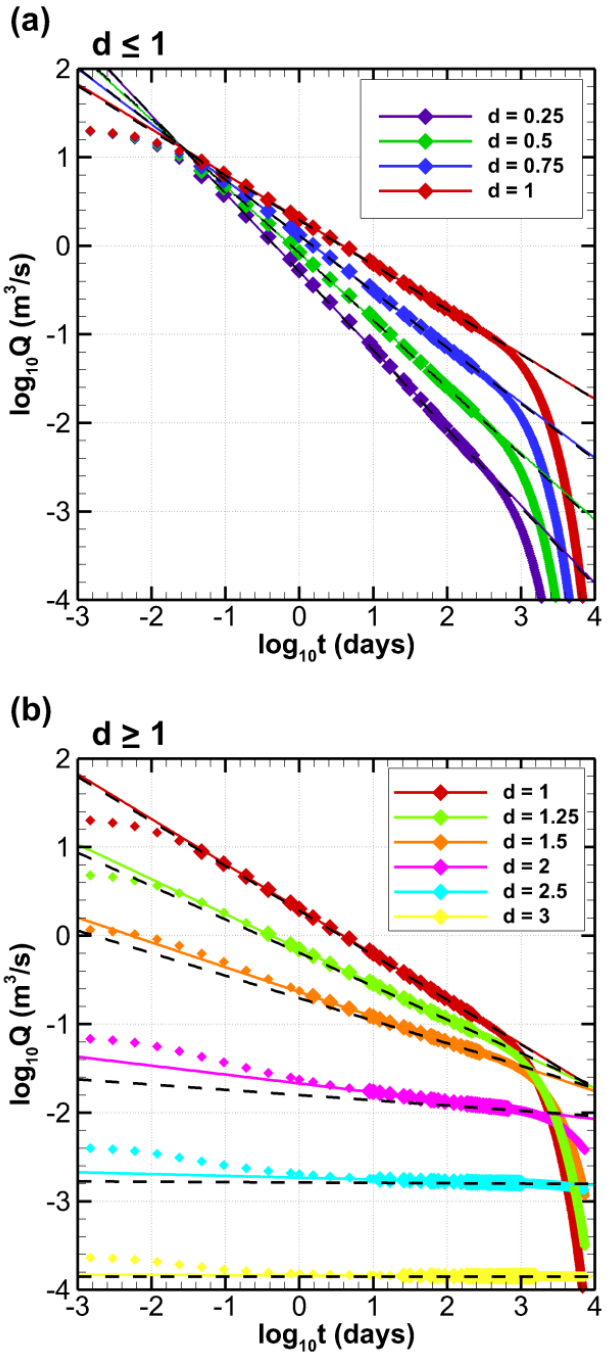

Figure 10 — Numerical simulation results showing production rate versus time for various flow dimensions *d*), for u_0 = 0.766. Symbols show simulation results; colored lines show linear fits to large symbols. Black dashed lines show linear fits to late-time simulation results for models with large radial extent.

To illustrate the Excel tool for *n* different from ½, we look again at the example problem shown in Section 3. The curve fit assuming *n* = ½, shown in Figure 6, over-estimates production corresponding to the first four time data points, but is very good for all times after 4 months. Very early data

are often ignored in the curve fitting analysis because they may be controlled by near-wellbore effects that are not accounted for in the idealized analytical solution. However, if the 1-4 month data shown in Figure 6 are considered reliable, they could be included in the fitting process by using a value of $n < ½$. Using the results of the $n = ½$ fit as initial guesses: $u_0 = 0.75$, $n = 0.5$, $t_0 = 16.5$, $Q_0 = 0.48$, and allowing n, t_0, and Q_0 to vary, the Solver returns a good fit for $n = 0.39$, $t_0 = 9.2$ years, and $Q_0 = 0.81$ (Figure 11) with a value of 0.34 for the objective function.

The physical interpretation of d and n can be summarized as follows:

- $d = 1$, $n = ½$: (original S&K case) well-connected fracture network in SRV, uniform primary fracture
- $d < 1$, $n > ½$: (mS&K case, steeper decline) sparse or poorly connected fracture network in SRV, uniform primary fracture
- $d > 1$, $n < ½$: (mS&K case, shallower decline) well-connected fracture network in SRV, heterogeneous primary fracture with only localized zones of high permeability

The essential difference between $n > ½$ and $n < ½$ is that for $n > ½$, there is a diverging geometry for the flow from the fracture network to the primary fracture, and for $n < ½$, there is a converging geometry. Figure 8 shows these diverging and converging flow geometries schematically. Figure 1 illustrates the fracture network that produces the linear flow geometry of the original S&K solution with $d = 1$ and $n = ½$.

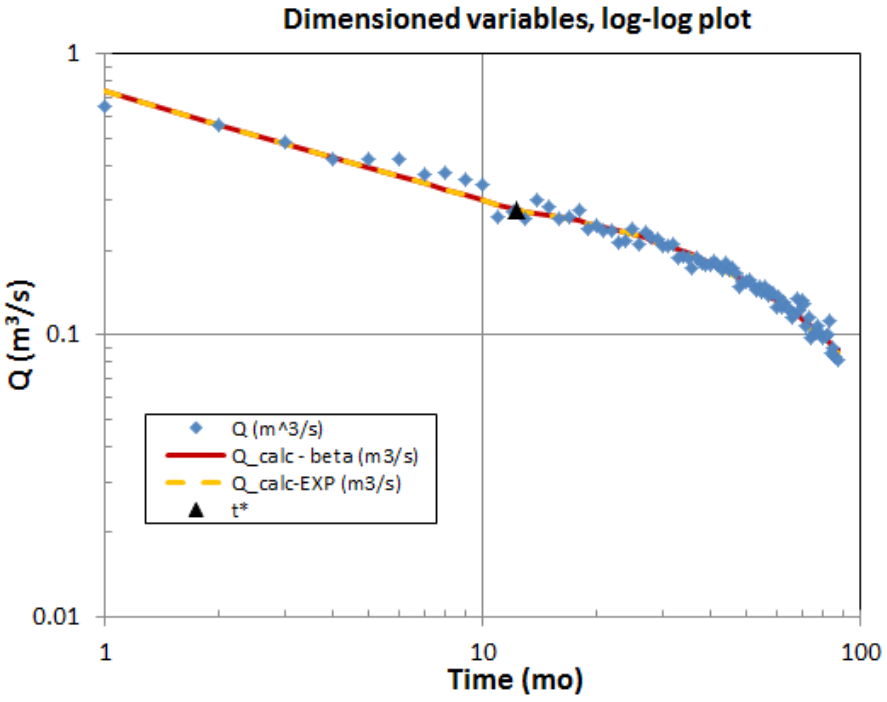

Figure 11—Step 1 curve-fit obtained by the Solver when n is allowed to vary along with Q_0 and t_0.

In summary, if field production data show a linear trend on a log-log plot of production rate versus time, then the absolute value of the slope n may be used to estimate the flow dimension d that is characteristic of the SRV. The concept of a single flow dimension being representative of an entire SRV is an extreme simplification, but one that may prove useful in predicting future production decline.

5. Conclusions

We have developed a simple, Excel-based tool for the analysis of the complex problem of gas production from a hydraulically fractured tight/shale gas reservoir, based on curve fitting a semi-analytical solution to production decline data. It is simple to use and can provide rapid estimates of the important parameters governing the system behavior, and it is scientifically robust as it incorporates the key features of hydraulically fractured gas reservoirs: gas is produced from a finite SRV consisting of a primary fracture and a secondary fracture network; exchange with adsorbed gas is also considered. The semi-analytical solution for production rate is bimodal, with a power-law decline for early times (before the outer boundary of the SRV is felt) and an exponential decline at later times. We generalized the original bimodal solution of Silin and Kneafsey (2012) so that the power-law exponent is a parameter n, rather than fixed at ½, to represent a broader range of fracture-network geometries and facilitate matching production decline curves that do not show a -½ slope at early times.

Curve fitting enables an improved understanding of the hydraulic fracturing process by estimating fracture geometry properties (A, D), SRV flow and transport properties (k_D, ϕ, A_s), and operational parameters (p_W, p_R). This understanding provides guidance for deployment of future stages and wells, thereby improving the efficiency of the hydraulic fracturing process, making it more economical and lessening its environmental impact.

Additional benefits include the ability to predict future production decline, including the productive lifetime of the stage. Moreover, the semi-analytical solution can provide verification for complex numerical models. Finally, the present approach, although designed for shale-gas production, should be adaptable to many gas-flow problems in dual-permeability media, whether hydraulically or naturally fractured or highly heterogeneous sedimentary rock, such as geothermal energy extraction, CO_2 storage, environmental remediation, and nuclear waste isolation.

Acknowledgements

We appreciate the scientific discussions with members of the Gas Technology Institute, particularly Xinya Xiong, Jordan Ciezobka, and Iraj Salehi. We thank Dmitriy Silin, Stefan Finsterle, Michael Hannon, and Tad Patzek for their reviews of an earlier version of this paper. This work was performed at Lawrence Berkeley

National Laboratory of the US department of Energy (DOE) under Contract No. DE-AC02-05CH11231. It was funded by the Research Partnership to Secure Energy for America (RPSEA) through the Ultra-Deepwater and Unconventional Natural Gas and Other Petroleum Resources program authorized by the US Energy Policy Act of 2005. RPSEA is a nonprofit corporation whose mission is to provide a stewardship role in ensuring the focused research, development, and deployment of safe and environmentally responsible technology that can effectively deliver hydrocarbons from domestic resources to the citizens of the US. RPSEA, operating as a consortium of premier US energy research universities, industry, and independent research organizations, manages the program under a contract with DOE's National Energy Technology Laboratory.

Nomenclature*

A area of SRV (m^2) [A]
A_s sorption group, $A_s = \rho_0 \rho_k S_k c_f/(c_g \phi)$ [As]
c_f gas desorption rate ($kg/(m^3 Pa)$) [cf]
c_g gas compressibility ($kg/(m^3 Pa)$), $c_g = M/(ZRT)$ [cg]
D half-thickness of SRV (m) [D]
d flow dimension [dim]
k_D permeability of SRV (m^2) [log10Kd]
M gas molar mass (kg/mol) [M]
n absolute value of early-time slope of the production decline curve
p pressure (Pa)
p_R reservoir pressure (Pa) [Pr]
p_W well pressure (Pa) [Pw]
Q production rate (m^3/s) [Q]
Q_0 characteristic production rate (m^3/s) [Q0]
Q_D dimensionless production rate, $Q_D = Q/Q_0$ [Qd]
R Universal gas constant ($m^3 Pa/(K\ mol)$) [Rgas]
r_p half-aperture of primary fracture (m) [rp]
S_k relative volume of kerogen [Sk]
T temperature (K) [T]
t time (s)
t_0 characteristic time (s) [t0, years]
t_1 earliest time that log-log production rate versus time plot is linear (s) [time1, mo]
t^* transition time (s) [tstar, mo]
u dimensionless pressure squared, $u = (p/p_R)^2$
u_0 dimensionless well pressure squared, $u_0 = (p_W/p_R)^2$ [u0]
Z gas compressibility factor [Z]
α parameter controlling early-time solution for Q [alpha]
β function controlling late-time solution for Q [beta]
ϕ porosity of SRV [phi]
μ gas viscosity (Pa·sec) [mu]
ρ_0 gas density at standard conditions (kg/m^3) [rho0]
ρ_k density of kerogen (kg/m^3) [rhok]
τ dimensionless time, $\tau = t/t_0$ [tau]
τ^* dimensionless transition time, $\tau^* = t^*/t_0$ [taustar]
ξ dimensionless distance

*Entries in square brackets show the variable name used in the CurveFit tab of the spreadsheet, where subscripts and Greek symbols are not used. If different units are used in the spreadsheet, they are shown.

References

Al-Ahmadi, H.A., A.M. Almarzooq, and R.A. Wattenbarger, Application of linear flow analysis to shale gas wells – field cases, SPE 130370, presented at the SPE Unconventional Gas conference, Pittsburgh, PA, USE, 23-25 February 2010.

Barker, J.A., A generalized radial flow model for hydraulic tests in fractured rock, *Water Resources Research*, 24(10), 1796-1804, 1988.

Cai, L., D.-Y. Ding, C. Wang, Y.-S. Wu, Accurate and efficient simulation of fracture-matrix interaction in shale gas reservoirs, *Transport in Porous Media*, 107, 305-320, 2015.

Cinco-Ley, H. and F. Samaniego, Transient pressure analysis for fractured wells, SPE 7490, *Journal of Petroleum Technology*, 33, 1749-1766, September 1981.

King, G. E., Hydraulic Fracturing 101: What every representative, environmentalist, regulator, reporter, investor, university researcher, neighbor and engineer should know about estimating frac risk and improving frac performance in unconventional gas and oil, in SPE 152596, SPE Hydraulic Fracturing Technology Conference, pp. 1–80, Society of Petroleum Engineers, Woodlands, TX, 2012.

Doughty, C., Generating one-column grids with fractal flow dimension, *Computers & Geosciences,* 108, 33-41, 2017.

Doughty, C. and G.J. Moridis, User's guide for the spreadsheet analysis of bimodal production decline curve in a hydraulically-fractured shale-gas reservoir, LBNL report in preparation, Lawrence Berkeley National Laboratory, Berkeley, CA, 2018.

Ilk, D., J.A. Rushing, A.D. Perego, and T.A. Blasingame, Exponential vs. hyperbolic decline in tight gas sands – understanding the origin and implications for reserve estimates using Arps' decline curves, SPE 116731, presented at 2008 SPE Annual Technical Conference and Exhibition, Denver, Colorado, USA, 21-24 September 2008.

Lunati, I. and S.H. Lee, A dual-tube model for gas dynamics in fractured nanoporous shale formations, *Journal of Fluid Mechanics*, 757, 943-971, 2014.

Oldenburg, C.O., G.J. Moridis, N. Spycher, and K. Pruess, EOS7C Version 1.0: TOUGH2 module for carbon dioxide or nitrogen in natural gas (methane) reservoirs, *Rep. LBNL-56589*, Lawrence Berkeley National Laboratory, Berkeley, CA, 2004.

Olorode, O.M., C.M. Freeman, G.J. Moridis, and T.A. Blasingame, High-resolution numerical modeling of complex and irregular fracture patterns in shale gas and tight gas reservoirs, SPE 152482, presented at SPE Latin American and Caribbean Petroleum Engineering Conference, Mexico City, Mexico, 16-18 April 2012.

Nobakht, M. and C.R. Clarkson, A new analytical method for analyzing linear flow in tight/shale gas reservoirs: constant-flowing-pressure boundary condition, SPE 143989, presented at Americas Unconventional Gas Conference, The Woodlands, Texas, USA, 12-16 June 2011.

Patzek, T.W., F. Male, and M. Marder, Gas production in the Barnett Shale obeys a simple scaling theory, *Proceedings, National Academy of Science*, 110(49), 19731-19736, 2013.

Patzek, T.W., F. Male, and M. Marder, A simple model of gas production from hydrofractured horizontal wells in shales, *AAPG Bulletin*, 98, 12, 2507-2529, 2014.

Press, W.H., B.P. Flannery, S.A. Teukolsky, and W.T. Vetterling, *Numerical Recipes: The art of scientific computing*, Cambridge University Press, New York, 1986.

Pruess, K., The TOUGH Codes—A Family of Simulation Tools for Multiphase Flow and Transport Processes in Permeable Media, *Vadose Zone Journal*, 3, 738-746, 2004.

Pruess, K., C. Oldenburg, and G. Moridis, TOUGH2 User's Guide, Version 2.0, *Rep. LBNL-43134*, Lawrence Berkeley National Laboratory, Berkeley, CA, 1999.

Silin, D. and T. Kneafsey, Shale gas: nanometer-scale observations and well modelling, SPE 149489, *J. Canadian Petroleum Technology*, 464-475, November 2012.

24
Wang, C., D. Ding, and Y.-S. Wu, Characterizing hydraulic fractures in shale gas reservoirs using transient pressure tests, SPE 163819, presented at SPE Hydraulic Fracturing Technology Conference, The Woodlands, Texas, USA, 4-6 February 2013.

Appendix A. Errata for Silin and Kneafsey (2012) SPE 149489

Equation (14) is two separate equations $\Psi(p)=\frac{1}{2}c_g p^2$

$$F'(p)=c_g$$

Equation (34) $$t_s \approx \left(1+\frac{\rho_0 \rho_k S_k c_f}{c_g \phi}\right)\frac{\mu \phi D^2}{k_D p_R}\frac{1}{\alpha^2}$$

Equation (35) $$Q(t)=2A\frac{c_g}{\rho_0}\sqrt{\left(\phi+\frac{\rho_0 \rho_k S_k c_f}{c_g}\right)\frac{k_D}{\mu p_R}}\frac{p_R^2-p_W^2}{\alpha\sqrt{t}}$$

Equation (36)

$$Q(t)=2Ac_g k_D \frac{(p¿¿R^2-p_W^2)}{\rho_0 \mu D}\exp\left[-3\frac{p_W}{p_R}\left(\frac{1}{\phi+\frac{\rho_0 \rho_k S_k c_f}{c_g}}\right)\frac{k_D p_R}{\mu D^2}t-\frac{1}{\alpha^2}\right]¿$$

Equation (A-14) $$-\int_0^\infty \left.\frac{\partial u}{\partial \xi}\right|_{\xi=0} d\tau=\frac{2}{3}\frac{(1-u_0)^{3/2}}{[\sqrt{u_0(1-u_0)}+\arcsin\sqrt{1-u_0}]}+\frac{2}{3}\frac{(1-u_0)}{\sqrt{u_0}}$$

Appendix B. Numerical Simulations of Gas Production Using One-column Grids with Different Flow Dimensions

A series of numerical simulations were done with the TOUGH2 code (Pruess et al., 1999; Pruess, 2004) using the equation of state module EOS7C (Oldenburg et al., 2004) to investigate gas production from a hydraulically fractured medium, for a range of flow dimensions for the network of fractures making up the SRV and the primary hydraulic fracture. TOUGH2 is a general purpose numerical simulator for multi-component, multi-phase fluid flow and heat transport through geologic media. In general, EOS7C includes components water, brine, methane, and carbon dioxide or nitrogen, which partition among aqueous, gaseous, and supercritical phases. Here we consider gaseous methane to be the only mobile fluid phase, with immobile water also present.

Grids with fractal dimension d = 0.25, 0.5, 0.75, 1, 1.25, 1.5, 2, 2.5, and 3 were created using a fractal grid generation method (Doughty, 2017) to model gas production from the stimulated reservoir volume surrounding a hydraulic fracture.

One end of the one-column grid (r = 0) is the primary fracture and the opposite end (r = D) is a no-flow boundary, to represent the outer limit of the SRV, beyond which permeability is assumed to be negligible. The length of the column (D = 150 m) and the number of grid blocks (300) are the same for each grid. For d < 1, the area of the primary fracture (at r = 0) is equal to the area of the SRV, A=31,416 m^2, and area decreases as r increases, to represent a sparse fracture network. In contrast, for d > 1, the area at r = D is set at A, and area decreases as r decreases to represent flow converging to the heterogeneous primary fracture.

To model gas production, the first grid block, which represents the primary fracture, is held at a constant pressure p_W lower than the reservoir pressure p_R, and the gas mass flow rate into that grid block Q is converted to volumetric flow rate at standard conditions by dividing by ρ_0. The thickness of the grid block is r_p, the half-aperture of the primary fracture. For comparison to the bimodal solution, the numerically simulated value of Q must be doubled to account for flow into both sides of the primary fracture. Porosity is 0.12 and permeability is 0.013 mD. Sorption is neglected by assuming S_k = 0. Initial conditions are P = 200 bar, T=28ºC, a methane saturation of 0.85, and a water saturation of 0.15 (with methane fully mobile and water immobile). Two cases were considered: u_0 = (p_W/ p_R)^2 = 0.766 and u_0 =0.25. While the bimodal solution assumes gas viscosity is constant, in the numerical simulations viscosity is pressure dependent, so using a large value of u_0 minimizes pressure differences, making a fairer comparison. Additionally, in the numerical simulations a small amount of methane is dissolved in the aqueous phase, some of which comes out of solution when pressure is lowered at the well. This effect is negligible for u_0 = 0.766 and still quite small for u_0 = 0.25. Thus, the aqueous phase plays no active role in the simulations, other than filling some of the pore space, so that the effective porosity of the numerical model for the gas phase is 0.12*0.85 = 0.102.